PEPT Study of Particle Cycle and Residence Time Distributions in a Wurster Fluid Bed

Liang Li
Dept. of Chemical and Biological Engineering, Chalmers University of Technology, SE-412 96 Gothenburg, Sweden

Pharmaceutical Development, AstraZeneca R&D, Mölndal, Sweden

Anders Rasmuson
Dept. of Chemical and Biological Engineering, Chalmers University of Technology, SE-412 96 Gothenburg, Sweden

Andy Ingram
School of Chemical Engineering, University of Birmingham, Edgbaston, Birmingham B15 2TT U.K.

Mats Johansson, Johan Remmelgas, Christian von Corswant, and Staffan Folestad
Pharmaceutical Development, AstraZeneca R&D, Mölndal, Sweden

DOI 10.1002/aic.14692
Published online November 28, 2014 in Wiley Online Library (wileyonlinelibrary.com)

Particle cycle and residence time distributions are critical factors in determining the coating quality in the Wurster process. Positron emission particle tracking experiments are performed to determine the cycle and residence times of particles in different regions of a Wurster fluid bed. The results show that particles tend to recirculate in and sneak out below from the Wurster tube. The experiments also show that a larger batch size leads to a shorter cycle time and a narrower cycle time distribution (CTD). It is possible to avoid recirculations and obtain a shorter cycle time and a narrower CTD by selecting the operating conditions appropriately or via equipment design. Experiments using binary mixtures of particles with a diameter ratio of 1.5 show that large particles have a longer cycle time than small particles and that the cycle time is shorter for mixtures with approximately equal amounts of small and large particles. © 2014 American Institute of Chemical Engineers *AIChE J*, 61: 756–768, 2015
Keywords: fluid bed, coating, cycle time, residence time distribution, positron emission particle tracking

Introduction

The Wurster process[1] is extensively used in industry to coat particles, granules, pellets, and similar materials.[2,3] It is used for chemical applications to provide controlled or delayed release properties in general and in the food industry to protect unstable ingredients, mask undesirable flavors, and modify the physical characteristics of foods.[2] In the pharmaceutical industry, it is typically used to deposit drug substances and functional films on, for example, particles, granules, and tablets in order to manufacture drug products or intermediates with functional properties controlling drug product release in the gastrointestinal tract.

The Wurster process is basically a fluid bed in which a coating solution in the form of small droplets is sprayed onto particles, as shown in Figure 1. The droplet spray is created using an air-assisted atomization nozzle that is mounted at the bottom of the bed. In addition to this atomization flow, a hot fluidization air flow is supplied through the bottom of the bed. This fluidization flow is supplied at a rate that keeps the particles near minimum fluidization, and serves to dry the wetted particles.

The fluid bed can be divided into several regions: the spray zone, the Wurster tube, the fountain region, the downbed region, and the horizontal transport region.[4–6] In an idealized view of the process, particles enter the spray zone at the center of the bed to receive an amount of coating solution. Particles then dry as they are carried upward through the Wurster tube by the atomization and fluidization flow, as the particles reach the fountain region, and as they settle down through the downbed and horizontal transport regions. When they approach the bottom of the vessel, they are ready to again enter the spray zone for the next coating event. This sequence of coating and subsequent drying is usually referred to as a cycle.

For functional films, a variability in the thickness of the film can have an effect on the rate of release of the drug substance. As the amount of coating deposited onto a particle depends on the number of times the particle passes the spray zone and on the amount of coating solution that the particle receives per pass, it is clear that the cycle time and the cycle time distribution (CTD) are important factors[7–10] in

Correspondence concerning this article should be addressed to A. Rasmuson at rasmuson@chalmers.se.

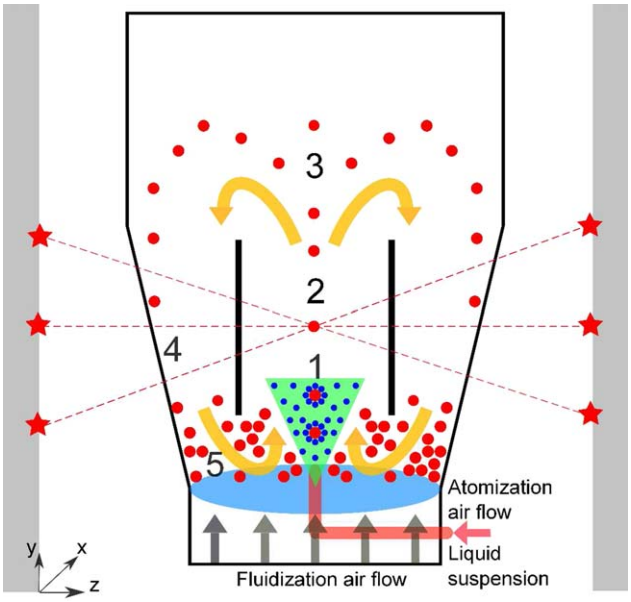

Figure 1. Schematic of the Wurster process and PEPT measurement system: (1) spray zone, (2) Wurster tube, (3) fountain region, (4) downbed region, and (5) horizontal transport region.

[Color figure can be viewed in the online issue, which is available at wileyonlinelibrary.com.]

determining the efficiency of the manufacturing process and the quality of the product. In the previous work, Mann and Crosby[11] measured the CTDs in spouted beds using radioactive and magnetic particles. A substantial reduction in the mean and variance of the CTD was observed, when a small amount of air was fed to the annular bed. Shelukar et al.[9] reported a decrease in the mean cycle time with an increase in the air flow rate or with an increase in the partition gap. In the work by San José et al.,[12] it was found that the draft tube narrows the CTDs of particles and that a higher horizontal transport region leads to a shorter mean cycle time. In addition, they made a summary of experimental results for cycle times from other studies.

Of course, the coating quality does not depend only on the coating thickness. For example, for functional films the coating quality can depend also on the drying rate of particles in the vessel. As shown by Karlsson et al.,[13] who studied the Wurster process by combining a detailed multiphase computational fluid dynamics (CFD) model with experimental work, a change in the process conditions influences the drying rate differently in different regions of the vessel. It is therefore of great interest to study not only the cycle time and the CTD but also the residence time distribution (RTD) of particles in different regions of the bed.

To determine the CTD and the RTD in different regions experimentally, it is necessary to employ a technique that can detect the motion of individual particles. Although this may seem straightforward, most experimental techniques, such as various imaging techniques, can only be used to probe particle motion near a surface. Fortunately, however, techniques based on labeled tracer particles exist that can be used to follow single particle trajectories in a noninvasive manner (almost) regardless of where in the bed the particles are. One such technique is the positron emission particle tracking (PEPT) technique, in which a radioactively labeled tracer particle is used. As the PEPT technique can be used to follow single particle trajectories, even in dense particulate systems, it is increasingly used for particulate flows. For example, work on the motion of tablets in a Wurster coating process using the technique has been reported by Fitzpatrick et al.[14] In addition, Barigou et al.[15] and Van de Velden et al.[16] applied the technique to determine the RTD in vertical and horizontal pipe flow and in a circulating fluidized bed (CFB) reactor, respectively. The technique was also used by Chan et al.[17] to aid the design of CFB-riser reactors.

The main objective of this work is to better understand the particle motion in Wurster fluid beds for particle coating by measuring the CTD and the RTD in different regions. Because the PEPT technique is well established and gives precisely the information that is of interest, this technique is employed. A series of PEPT experiments in which the process conditions are varied are conducted on a laboratory-scale Wurster bed, and the measured particle trajectories are then used to determine the CTD and the RTD in different regions of the bed. In an effort to shed light on the underpinning mechanisms by which the coating thickness changes, experimental results on the CTD are obtained for mixtures of particles with two different sizes. These results can also give further insight into the general and detailed flow behavior of particles in Wurster beds.

As a related objective, these data will be used in a subsequent study to validate CFD-DEM (i.e., discrete element method) computational models for particle motion in fluid beds. As the computational effort for these models depends to a great extent on the number of particles in the simulation, care is also taken in this PEPT study to focus on systems with limited numbers of particles, and to employ processing conditions that may be simulated in a reasonable time.

Materials and Methods

The PEPT technique

In a PEPT measurement system, a radioisotope is incorporated into a tracer particle. The radioisotope decays in beta-decay as the tracer particle moves around in the fluid bed. Back-to-back γ-rays, that is, γ-rays that travel in opposite directions, are then emitted. The γ-rays are detected via two large position sensitive detectors, as shown in Figure 1. Two events that are detected simultaneously are used to define the so-called line of response (LOR), that is, a line along which the tracer particle is located. Triangulation of successive LORs can then be used to find the location of the tracer particle. In practice, a few hundred LORs are used for each location. More details about the technique and algorithms can be found in the work by Parker et al.[18–20]

Materials

In this work, microcrystalline cellulose (MCC) spheres with a volume mean diameter (VMD) of 1749 and 2665 μm (see photograph of samples in Figure 2), were manufactured on request by Umang Pharmatech Pvt. The material properties are given in Table 1. These MCC spheres are relatively large in order to limit the number of particles and the computational cost in future modeling studies.

A number of particles in each size range were selected for radioactive labeling; a scanning electron microscope was

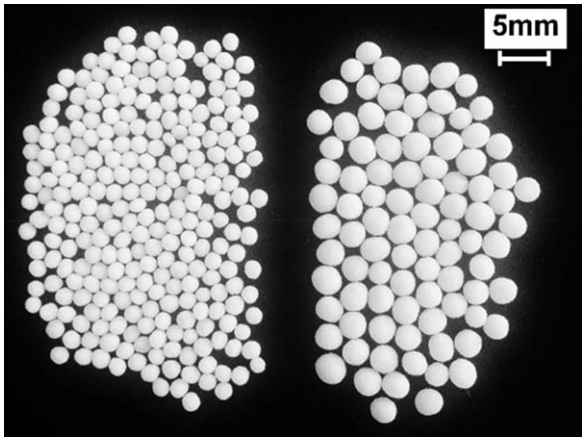

Figure 2. Photograph of samples of the 1749 and 2665 μm MCC spheres.

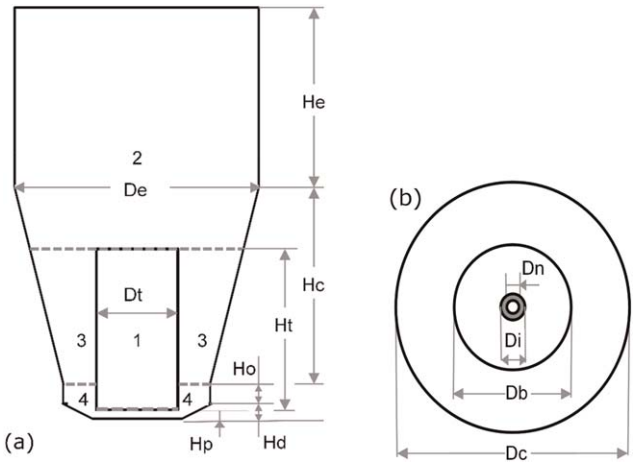

Figure 3. The dimensions of the Wurster bed, (a) side view showing the different regions: (1) Wurster tube, (2) fountain region, (3) downbed region, and (4) horizontal transport region; (b) top view.

used to select tracer particles with a diameter that was approximately equal to the VMD. Tracer particles are labeled with Fluorine-18. Fluorine-18 is an ideal radioisotope because its half-life of 109 min allows for run times of several hours combined with almost complete deactivation in 24 h, thus eliminating any risk of equipment contamination. Also, the decay is 100% beta-plus, so there are no additional gamma photons to corrupt the data. Fluorine-18 is produced by direct irradiation of water with 3He ions using a Scanditronix MC40 Cyclotron. The irradiation generates free $18F^-$ in the water which is then transferred to the tracer particle by simple absorption and adsorption through immersion for about 30 min.

For each run, only one tracer particle was incorporated into the fluid bed. Since the activity of the tracer particle lasted for approximately 6 h and a typical experiment took approximately 1.5 h, the same tracer particle could be used for several experiments. The tracer activity decreased during the experiments, so that it was necessary to move the detectors closer together between experiments in the same series in order to compensate for the decreased activity of the tracer particle.

Equipment and procedures

The dimensions of the fluid bed are illustrated in Figure 3 and Table 2. It is noted that the nozzle does not generate swirl. The opening at the center of the bowl-shaped distributor plate covers the entire base and has a diameter of 52 mm. The orifices below the annulus have a diameter of 3 mm and in total take 4% of the area. The origin of the PEPT measurement system is located in a corner of a detector. To establish a reference point for the PEPT camera data points, the tracer particle was positioned at marked points on top of the Wurster tube, so that the center of the tube outlet can be identified. As all geometric dimensions are known, it was then possible to identify the center of the bottom of the bed.

Prior to the experiments, a series of preliminary experiments were performed to estimate the operating conditions, for example, the air flow, which plays a key role in circulating the particles in the fluid bed. As the particle motion was very sensitive to the air flow supplied in the bed, the values that gave stable particle dynamics were finally used. In addition, preliminary DEM simulations were carried out to ensure that the chosen operating conditions and number of particles may be simulated in a reasonable time. For a typical run, 200 g 1749 μm almost monosize particles were used, while for study of mixtures, 25, 50, and 75% of 200 g 1749 μm particles were replaced by 2665 μm particles. A summary of configuration and operating parameters for each run is listed in Table 3. A base case, run #2, was set to the middle level of each variable.

Postprocessing of PEPT data

The raw data from the PEPT measurements consist of the coordinates of the tracer particle at different points in time. As shown in Figure 1, x and z are the coordinates in the horizontal directions relative to the axis of the bed, and y is the axial distance measured from the bottom of the bed. An example of a measured particle trajectory is shown in Figure 4a.

In practice, there is a degree of corruption of data arising from Compton scattering of the photons or incorrect pairing. This corruption must be dealt with using a statistical algorithm, as it does not give the correct information about the particle location. In this work, we use the algorithm

Table 1. Summary of the Particle Properties

Item	Volume Mean Diameter[a] (μm)	Surface Mean Diameter (μm)	Particle Density[b] (kg/m^3)	Terminal Velocity[c] (m/s)
1	1749	1740	1420	7.8
2	2665	2651	1387	9.3

[a]The particle size was measured using a QICPIC Particle Size Analysis (Sympatec GmbH), at AstraZeneca R&D.
[b]The particle density was determined using mercury intrusion porosimetry (Micromeritics AutoPore III 9410) at Swerea IVF AB.
[c]The air property used in this calculation is determined at the room temperature, 20°C.

Table 2. The Dimensions of the Wurster Bed

Variable	Value
Diameter of expansion chamber, D_e (mm)	250
External diameter of the Wurster tube, D_t (mm)	50
Upper diameter of bowl distributor plate, D_c (mm)	114
External diameter of the base of bowl distributor plate, D_b (mm)	52
Internal diameter of the base of bowl distributor plate, D_i (mm)	12
Diameter of nozzle, D_n (mm)	5
Height of expansion chamber, H_e (mm)	160
Height of truncated cone, H_c (mm)	220
Height of the Wurster tube, that is, tube length, H_t (mm)	100, 150, 200
Height of the connection between bowl distributor and truncated cone, H_o (mm)	20
Height of bowl distributor, H_d (mm)	17
Height of partition gap, H_p (mm)	10, 15, 20

developed by Parker et al.[18] to discard the γ-rays that have been corrupted by scattering. This algorithm involves setting several parameters so as to obtain more reliable tracer locations, and once appropriate values of these parameters are found, it is straightforward to convert the raw data into physical coordinates in a Cartesian coordinate system with its origin at the center of the bottom of the bed. It is noted that it is difficult to detect the γ-rays, if there is too much metal between the tracer particle and the detector. For the present equipment, this occurs when the particle is below the connection between the truncated cone and the bowl distributor, approximately 40 mm above the bottom (see Figure 4a).

As no liquid suspensions were used in the experiments, a spray zone is not identified in this study. The Wurster bed is then divided into four different regions as illustrated in Figure 3. A cycle thus starts when the tracer particle appears in the Wurster tube and ends when it reappears in the Wurster tube, after having traveled through the Wurster tube and the fountain, downbed, and horizontal transport regions. When one cycle ends, another one begins. By following the trajectories of a tracer particle, two types of the trajectories are defined as follows (e.g., Figures 4b, c):

a. Cycle: the tracer particle departs from the spray zone, accelerates in the Wurster tube, and returns to the spray zone after passing through the fountain, downbed, and horizontal transport regions. An example of a cycle may be seen in Figure 4a at approximately 10 s and Figure 4b.
b. Recirculation: the tracer particle recirculates within the Wurster tube without passing through the downbed region. This type of trajectory is not desired because it is believed to increase the risk for agglomeration of particles and give a broader film thickness distribution. An example of a recirculation may be seen in Figure 4a at approximately 60 s and Figure 4c.

In defining these two types of trajectories, it must be pointed out that a cycle may or may not include recirculations. When a cycle does not have any recirculation, it is an ideal cycle. The mean values of cycle time for these cycles and ideal cycles are summarized in Table 4. Table 4 also shows the residence time of the particle in the Wurster tube and the fountain height, defined as the largest height the tracer particle reaches in a cycle. The residence time of the tracer particle in the different regions is calculated by measuring the time that the tracer particle spends in the corresponding regions. The RTD in the Wurster tube and the fountain, downbed, and horizontal transport regions is thus obtained in the same way as the CTD.

The run time

The run time that is required in order to detect a sufficient number of cycles can be expected to depend on the system. To determine the appropriate run time for the present system, the mean cycle time and the number of cycles were evaluated as functions of the run time. The result for the first run shows that the mean cycle time reaches a reasonably steady value of approximately 8.0 s after 2000 s or 200 cycles. In addition, the CTDs sampled from different numbers of cycles were compared as shown in Figure 5. Figure 5 shows that there are differences between the CTDs calculated based on 100 cycles and 250 cycles, but the distribution shapes are generally quite similar. After 500 cycles (i.e., 4000 s), the CTD is fairly steady with a mean cycle time of

Table 3. The Configuration and Operating Parameters for Each PEPT Run

Run#	Partition Gap (mm)	Batch Size (g)	Tube Length (mm)	Mass of 1749 μm Particles (g)	Mass of 2665 μm Particles (g)	VMD of Tracer Particle (μm)	Fluidization Air Flow Rate (m^3/h)	Atomization Air Flow Rate (m^3/h)	Run Time (h)
1	10	200	150	200	–	1749	73.3	3.50	3
2	15	200	150	200	–	1749	73.3	3.50	1.5
3	20	200	150	200	–	1749	73.3	3.50	1.5
4	15	400	150	400	–	1749	73.3	3.50	1.5
5	15	600	150	600	–	1749	73.3	3.50	1.5
6	15	200	100	200	–	1749	73.3	3.50	1.5
7	15	200	200	200	–	1749	73.3	3.50	1.5
8	15	200	150	–	200	2665	80.3	4.32	1.5
9	15	200	150	150	50	1749	80.3	4.32	1.5
10	15	200	150	150	50	2665	80.3	4.32	1.5
11	15	200	150	100	100	1749	80.3	4.32	1.5
12	15	200	150	100	100	2665	80.3	4.32	1.5
13	15	200	150	50	150	1749	80.3	4.32	1.5
14	15	200	150	50	150	2665	80.3	4.32	1.5
15	15	200	150	200	–	1749	65.8	3.50	1
16	15	200	150	200	–	1749	80.3	3.50	1
17	15	200	150	200	–	1749	73.3	2.49	1
18	15	200	150	200	–	1749	73.3	4.54	1

Run #2 is the base case for which each variable is at its middle level.

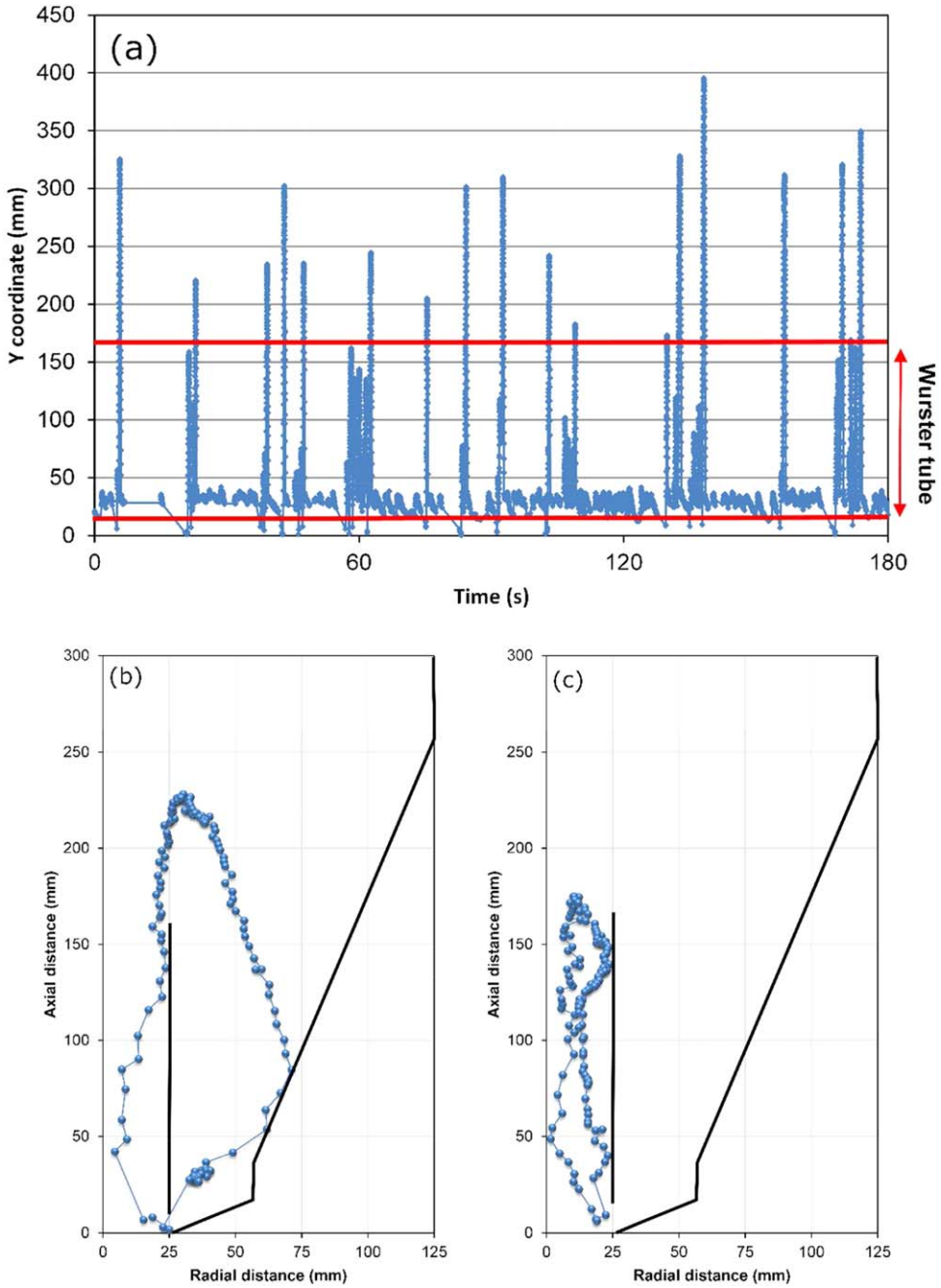

Figure 4. Examples of particle trajectories: (a) axial position above the bottom of the bed, and different types of trajectories (the bold lines are walls of the bed and Wurster tube), (b) cycle, and (c) recirculation.

[Color figure can be viewed in the online issue, which is available at wileyonlinelibrary.com.]

7.7 s. Thus, the conclusion drawn here is that 500 cycles or a run time of 1.5 h is sufficient to get a reliable CTD. Unless otherwise stated, a run time of 1.5 h was therefore used.

Effect of sampling interval

When the postprocessing parameters used to remove corrupt data are changed, the number of data points as well as the sampling interval, that is, the time resolution, also changes. It is therefore important to understand the effect of the sampling interval on the results. The dependence of the mean cycle time on the mean sampling interval is therefore investigated, as shown in Figure 6. The result shows that either a too small or too large sampling interval leads to visible differences in the mean values of cycle time. A small sampling interval is typically obtained using a small number of LORs, which results in insufficient statistics and thus a lower reliability. A large sampling interval, on the other hand, reduces the number of data points and decreases the time resolution considerably. To keep approximately the same time resolution for different configurations and operating parameters, the sampling interval employed was in the range 50–80 ms. It must be emphasized that Figure 6 only shows the mean sampling interval; the tracer particle location is sampled more frequently in the Wurster tube, while the sampling interval typically is much larger when the tracer particle moves in the lower bed (see Figure 4a).

Table 4. Summary of the Mean Cycle Time, Fountain Height, and Solids Flow Rate for Each PEPT Run

Run #	Number of Cycles	Mean Cycle Time[a] (s)	RSD of Mean Cycle Time (%)	Mean Fountain Height[b] (mm)	Mean Residence Time in the Wurster Tube[c] (s)	Fraction of Residence Time in the Wurster Tube in Cycle Time[d] (%)	Percentage of the Ideal Cycles (%)	Mean Cycle Time for the Ideal Cycles[e] (s)	RSD of Mean Cycle Time for the Ideal Cycles (%)	Mean Residence Time in the Wurster Tube for the Ideal cycles (s)	Mean Fountain Height for the Ideal Cycles (mm)	Mean Cycle Time for the Nonideal Cycles (s)	Mean Residence Time in the Wurster Tube for the Nonideal cycles (s)	Solids Flow Rate[f] (kg/s)	Solids Loading in the Wurster Tube[g] (kg/m^3)	Mass of Particles in the Wurster Tube[h] (g)
1	1396	7.70	98	232.4	1.35	17.5	35.6	4.10	73	0.46	233.9	9.70	1.84	0.0260	129.1	35.1
2	533	10.14	77	236.2	1.38	13.6	10.3	3.06	65	0.52	242.5	10.96	1.48	0.0197	100.3	27.2
3	575	9.45	70	218.2	1.55	16.4	5.6	2.77	44	0.48	216.0	9.85	1.62	0.0212	121.2	32.9
4	824	6.53	76	236.2	0.96	14.7	35.2	2.94	53	0.39	242.3	8.48	1.27	0.0613	216.9	58.9
5	1122	4.86	53	251.1	0.53	10.9	44.0	3.51	47	0.26	256.5	5.92	0.74	0.1235	240.7	65.3
6	1078	4.97	86	201	0.76	15.3	28.7	2.10	36	0.35	208.7	6.13	0.92	0.0402	168.7	30.5
7	221	24.28	88	248.8	5.03	20.7	2.7	5.35	22	0.43	250.7	24.81	5.16	0.0082	114.5	41.4
8	796	6.74	80	240	1.20	17.8	37.6	4.13	68	0.45	236.6	8.32	1.65	0.0297	130.9	35.5
9	1120	4.85	78	275.8	0.94	19.4	45.9	3.23	74	0.41	273.6	6.23	1.39	0.0372	142.6	38.7
10	683	7.94	123	286.7	0.95	12.0	37.8	2.72	57	0.45	290.9	11.11	1.26		88.4	24.0
11	1100	4.95	73	275.3	0.93	18.7	46.9	3.22	51	0.38	269.8	6.48	1.41	0.0370	137.8	37.4
12	904	5.95	96	267.1	1.02	17.1	33.1	2.74	44	0.42	274.4	7.53	1.31		125.9	34.2
13	884	6.09	73	254.1	1.11	18.3	38.6	3.56	48	0.42	251.6	7.68	1.55	0.0321	134.8	36.6
14	867	6.29	89	241.7	1.11	17.6	58.8	4.83	83	0.49	240.5	8.37	1.98		129.6	35.2
15	260	13.56	150	204.3	2.71	20.0	10.0	12.40	242	1.99	195.6	14.22	3.12	0.0147	147.4	40.0
16	633	6.14	90	253	1.00	16.3	55.3	4.84	99	0.50	249.1	7.74	1.61	0.0326	119.8	32.5
17	23	148.19	109	184.3	42.45	28.6	–	–	–		–	148.19	42.45	0.0013	211.1	57.3
18	942	5.61	80	288.1	0.90	16.0	49.4	3.92	75	0.40	290.8	7.26	1.38	0.0356	118.0	32.0

[a]Mean cycle time $\overline{t_c}=\frac{\sum_{i=1}^{n_c} t_{c_i}}{n_c}$, where t_{c_i} is the cycle time of the i^{th} cycle, and n_c is the number of cycles.

[b]Mean fountain height $\overline{h_c}=\frac{\sum_{i=1}^{n_c} h_{c_i}}{n_c}$, where h_{c_i} is the fountain height of the i^{th} cycle, and $h_{c_i}=y_{max_i}$, where y_{max_i} is the maximum axial distance from the distributor plate within the i^{th} cycle.

[c]Mean residence time in the Wurster tube $\overline{t_{r2}}=\frac{\sum_{i=1}^{n_c} t_{r2_i}}{n_c}$, where t_{r2_i} is the residence time of particles in the Wurster tube within the i^{th} cycle.

[d]Mean fraction of residence time in the Wurster tube in cycle time $\overline{p_{r2}}=\frac{\sum_{i=1}^{n_c}\left(\frac{t_{r2_i}}{t_{c_i}}\right)}{n_c}$.

[e]Mean cycle time for the ideal cycles $\overline{t_{cl}}=\frac{\sum_{i=1}^{n_{ci}} t_{ci_i}}{n_{ci}}$, where t_{ci_i} is the cycle time of the i^{th} ideal cycle, and n_{ci} is the number of ideal cycles.

[f]Solids flow rate in the bed $S=\frac{M}{t_c}$, where M is the batch size. For the mixtures, that is, runs# 9 and 10, runs# 11 and 12, and runs# 13 and 14, mass weighted average is made.

[g]Solids loading in the Wurster tube $S_{r2}=\frac{M\overline{t_{r2}}}{\overline{t_c}V_2}$, where V_2 is the volume of the Wurster tube.

[h]Mass of particles in the Wurster tube $M_{r2}=\frac{M\overline{t_{r2}}}{\overline{t_c}}$.

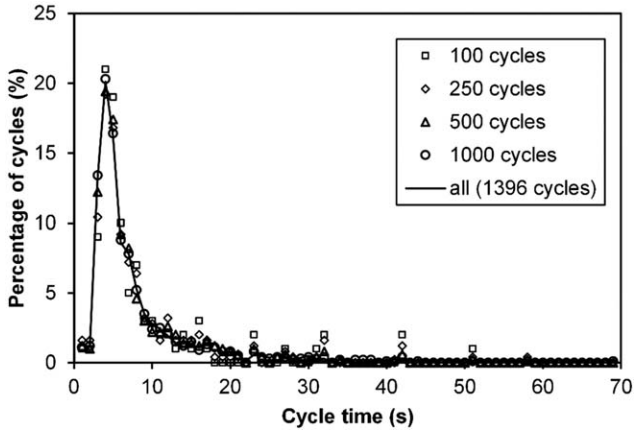

Figure 5. The cycle time distributions for run #1 sampled from varying numbers of cycles (partition gap 10 mm, batch size 200 g, particle VMD 1749 μm, tube length 150 mm, fluidization air flow rate 73.3 m^3/h and atomization air flow rate 3.50 m^3/h).

Results and Discussion

In this section, we present results from the PEPT studies. The presentation first focuses on a discussion about the general motion of particles with particular emphasis on the base case (run #2), that is, the experiment that corresponds to the center point of our experimental design. Following this discussion, we examine the effect of the operating conditions on the experimental results. Lastly, we discuss the cycle time for the mixtures of particles with different sizes.

General particle movement

Figure 7 shows the locations of the tracer particle in the fluid bed in the *z* and *y* directions (from which trajectories can be inferred) for the base case (run #2). The particle trajectories agree well with the behavior that is expected for a typical Wurster fluid bed. The mean cycle time is 10.14 s. The RTDs in the Wurster tube, the fountain, the downbed, and the horizontal transport regions are shown in Figure 8,

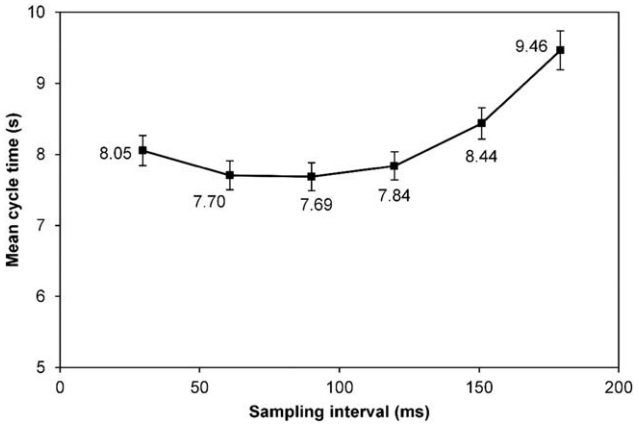

Figure 6. The effect of the mean sampling interval on the mean values of cycle time for run #1 (partition gap 10 mm, batch size 200 g, particle VMD 1749 μm, tube length 150 mm, fluidization air flow rate 73.3 m^3/h, and atomization air flow rate 3.50 m^3/h).

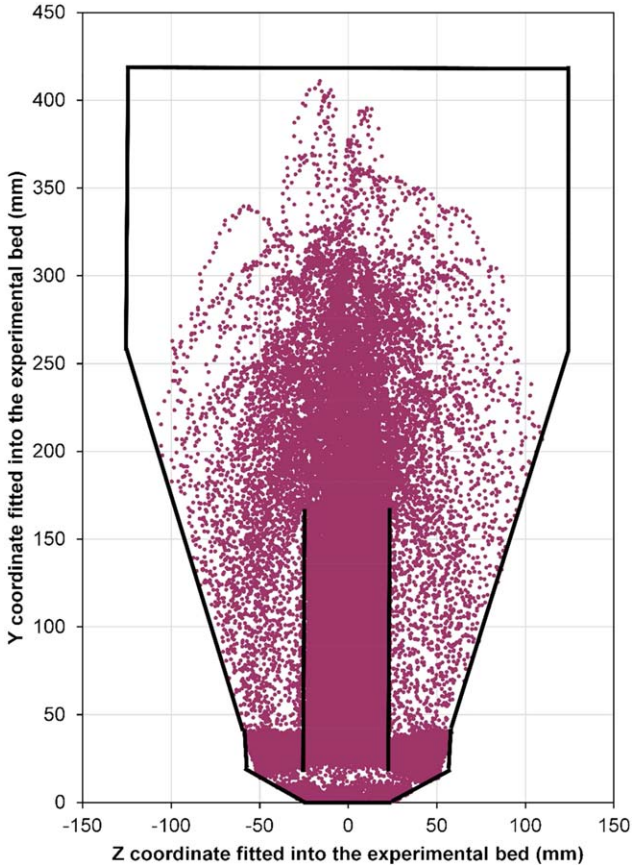

Figure 7. The particle movement in the Wurster bed for the base case (run #2) (partition gap 15 mm, batch size 200 g, particle VMD 1749 μm, tube length 150 mm, fluidization air flow rate 73.3 m^3/h, and atomization air flow rate 3.50 m^3/h).

[Color figure can be viewed in the online issue, which is available at wileyonlinelibrary.com.]

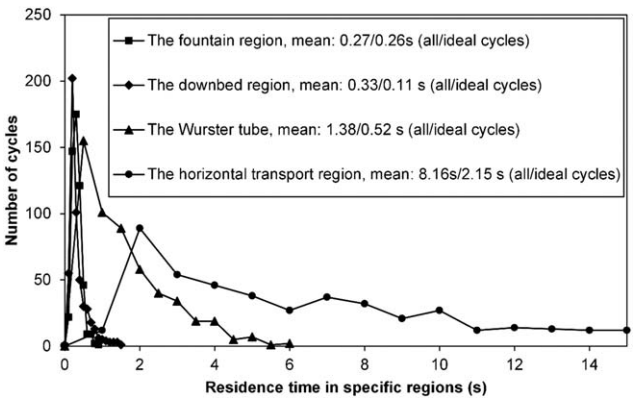

Figure 8. Residence time distributions in specific regions, with mean values of all cycles and ideal cycles provided, for the base case (run #2) (partition gap 15 mm, batch size 200 g, particle VMD 1749 μm, tube length 150 mm, fluidization air flow rate 73.3 m^3/h, and atomization air flow rate 3.50 m^3/h), the bin value for the fountain and downbed regions: 0.1 s, for the Wurster tube: 0.5 s, and for the horizontal transport region: 1 s.

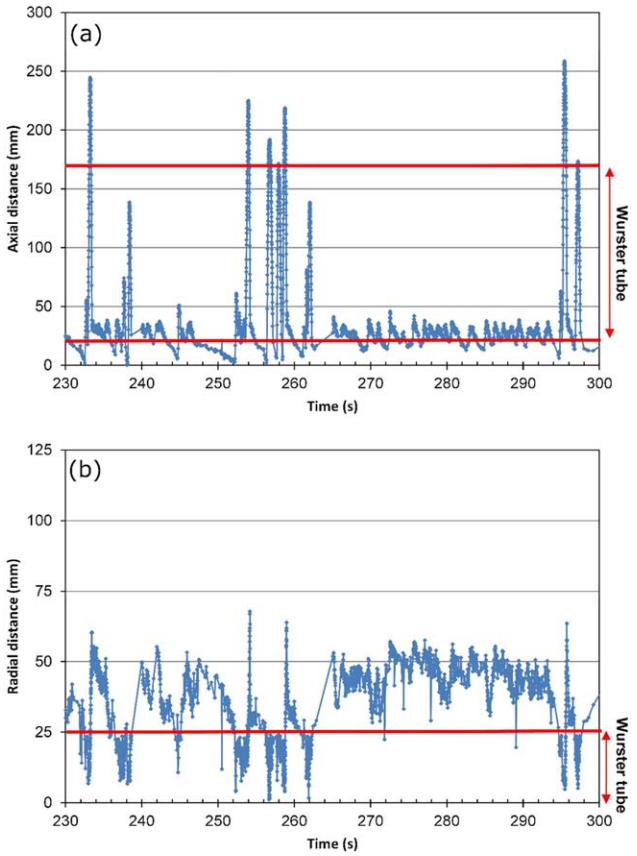

Figure 9. An example of the axial (a) and radial (b) position of a tracer particle during 230–300 s.

[Color figure can be viewed in the online issue, which is available at wileyonlinelibrary.com.]

along with the mean residence times. At these particular experimental conditions, the particle on average spends 1.38 s in the Wurster tube, 0.27 s in the fountain region, and 0.33 s in the downbed region. Prior to starting the next cycle, the particle then spends 8.16 s in the horizontal transport region. The RTD in the fountain region is quite narrow, while the widest RTD is obtained in the horizontal transport region; this wide RTD has a long tail that is not fully shown in Figure 8 (the longest residence time in the horizontal transport region is 44.39 s). The long mean residence time and wide RTD in the horizontal transport region is a result of the relatively low solids flow rate. A low solids flow rate coupled with an air flow that keeps particles fluidized results in a particle trajectory becoming more chaotic, and this random motion of a particle results in a long mean residence time and a wide RTD.

Results are obtained for the mean cycle time, the mean fountain height, the mean cycle time of the ideal cycles, and the mean residence time in the Wurster tube for all the runs. For the mean cycle time and the mean cycle time of the ideal cycles, the relative standard deviation (RSD) in the cycle time is also calculated. In addition, the solids flow rate in the fluid bed, the solids loading, and the mass of particles in the Wurster tube are estimated. The results are summarized in Table 4.

The mean cycle time in all runs, expect for runs #7 and 17, varies within the range of 4.8–13.6 s. For run #17, the one with a lower atomization air flow rate of 2.49 m^3/h, a cycle time of about 150 s is obtained, while the experimental conditions for run #7 (with a longer Wurster tube of 200 mm) result in a cycle time of 24.3 s. As mentioned previously, ideal cycles are desirable since a particle then has enough time to dry before it receives more spray droplets in the next coating cycle, thus avoiding the risk for agglomeration of the particles. In Table 4, it is shown that ideal cycles have a shorter cycle time as well as a narrower CTD (manifested by the lower RSD), which is beneficial for the coating uniformity. Table 4 also shows that the fraction of ideal cycles varies between 0 and 59% and that a large batch size, high fluidization air flow rate, and high atomization air flow rate give a large fraction of ideal cycles. By contrast, a large partition gap or a long Wurster tube results in very few ideal cycles, while no ideal cycles at all were obtained for the low atomization air flow rate.

One may observe in Table 4 that the difference of the residence time in the Wurster tube out of all cycles and that of the ideal cycles cannot explain the difference in the cycle time of all cycles and that of the ideal cycles. For example, the difference of the cycle time of all cycles and that of the ideal cycles for the base case is 7.06 s, while the residence time in the Wurster tube is only 1.38 s. This fact suggests that particles in nonideal cycles must spend a much longer time somewhere else, for example, in the horizontal transport region, than in the Wurster tube compared to particles in ideal cycles. To be specific, as shown in Figure 8, the difference in the residence time between all cycles and the ideal cycles in the fountain and downbed regions and in the Wurster tube is 0.01, 0.22, and 0.86 s, respectively, while the difference in the residence time in the horizontal transport region is 6.01 s. By closely examining particle trajectories, it is found that a particle in a nonideal cycle sometimes settles down in the Wurster tube and moves from the Wurster tube back to the horizontal transport region and then spends much more time in this region prior to starting the next cycle (see e.g., Figure 9 approximately at 238 and 263 s). Being able to identify this pattern of motion and the conditions under which it is more likely to happen is of great importance, as it implies that particles return to the horizontal transport region before being dried, which increases the risk for

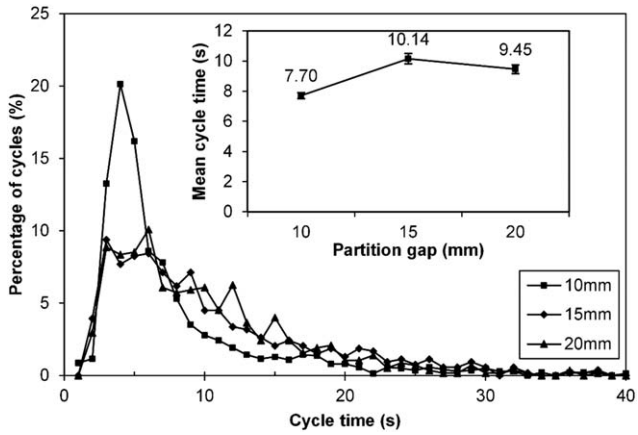

Figure 10. The CTDs and the mean values of the cycle time for runs #1, 2, and 3 with varying partition gaps (batch size 200 g, particle VMD 1749 μm, tube length 150 mm, fluidization air flow rate 73.3 m^3/h, and atomization air flow rate 3.50 m^3/h).

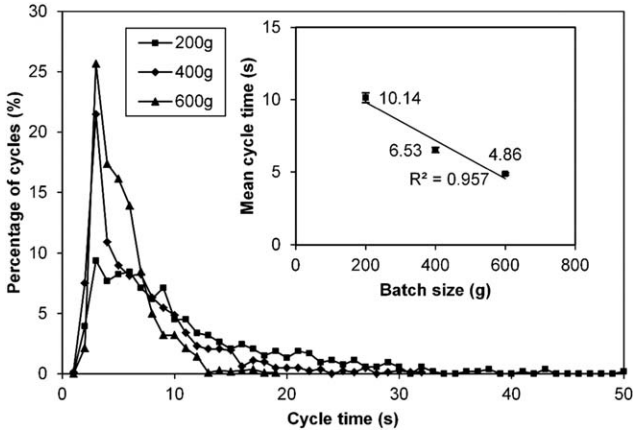

Figure 11. The CTDs and the mean values of the cycle time for runs #2, 4, and 5 with varying batch sizes (partition gap 15 mm, particle VMD 1749 μm, tube length 150 mm, fluidization air flow rate 73.3 m^3/h, and atomization air flow rate 3.50 m^3/h).

agglomeration. Specifically, the percentage of ideal cycles that indicates the probability of particles sneaking out from below the Wurster tube is shown in Table 4 and discussed in relevant subsections.

In the present study, the main objective is to examine the CTDs and RTDs, but the general information about the particle movement shown here for the base case is available for all runs. In the following subsections, where the effects of different geometric configurations and operating parameters are investigated in more detail; the detailed particle motion is therefore only presented if it is relevant to the discussion.

Effect of partition gap

The effect of the partition gap was studied for the batch size of 200 g at three different partition gaps: 10, 15, and 20 mm. The mean cycle time increases from 7.70 to 10.14 s when the partition gap increases from 10 to 15 mm (see runs #1 and 2 in Table 4). Further increasing the partition gap from 15 to 20 mm (run #3) leads to a slight decrease (by 0.69 s) in the mean value. Furthermore, Figure 10, which shows the CTDs for different partition gaps, clearly shows a higher percentage of shorter cycles for a partition gap of 10 mm, compared to a partition gap of 15 or 20 mm.

For very small partition gaps, the geometry of the vessel restricts the solids flow into the Wurster tube.[21] Increasing the partition gap has two effects[21,22]: it allows more particles to be transported into the Wurster tube simply by increasing the separation between the bottom plate and the Wurster tube but also causes some of the air from the center of the bottom plate to bypass the Wurster tube and instead flow through the downbed region. The latter effect results in a reduction of air flow rate in the Wurster tube and consequently less acceleration of the particles, which increases the risk for recirculation in the Wurster tube. Further increasing the partition gap may induce a transition of the behavior in the horizontal transport and downbed regions of the bed from a packed to a bubbling fluid bed,[6] which further decreases the solids flow into the Wurster tube. The increase in mean cycle time (and decrease in the solids flow rate) that is observed when the partition gap is increased from 10 to 15 mm indicate that for the particles used in this study the change in air flow is the dominating effect. This is further emphasized by the marked decrease in the percentage of ideal cycles which changes from 35.6% for the 10-mm gap to 10.3% for the 15-mm gap and to only 5.6% for the 20-mm gap. The observed decrease in mean cycle time for the ideal cycles with an increase in the partition gap may seem to contradict this conclusion but may be explained by noting that the decrease in the fountain height for the ideal cycles (233.9 mm at 10 mm, 242.5 mm at 15 mm, and 216.0 mm at 20 mm) results in a shorter flight time. This observation suggests that the partition gap should be kept just a bit larger than the value that eliminates the limitation of the solids flux for a certain batch size, if a short cycle time is required.

Effect of batch size

Figure 11 shows the effect of batch size on the cycle time. It is interesting to note that when the batch size increases by a factor of 3 (from 200 to 600 g) the mean cycle time decreases from 10.14 to 4.86 s, and the solids flow rate increases by a factor of approximately 6 (from 0.0197 to 0.1235 kg/s). As the solids flow rate increases more than the batch size, this result suggests that in practice a bigger batch can be processed in a shorter time provided the spray rate can be increased accordingly. In addition, a larger batch size is also observed to result in a narrower CTD, which is preferable as it implies less variability in the coating thickness between the individual particles.

One may think that increasing the batch size and thus increasing the bed height increases the flow resistance in the downbed region and that particles therefore should spend a longer time in this region. Indeed, Fitzpatrick et al.[14] observed that the cycle time increases when the batch size increases in their study of the motion of tablets in a Wurster coating process. In this study, however, a detailed examination of the cycle time reveals that it decreases approximately linearly with an increase in the batch size. A similar linear relationship between the cycle time and the batch size was found by San José et al.[23] in a conical spouted bed and by Chan et al.[24] in a Wurster coater. In some cases, this effect may be caused by an increased "hydrostatic pressure" due to

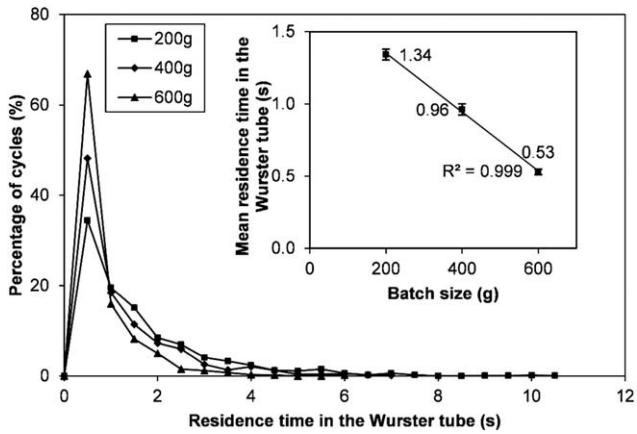

Figure 12. The RTDs in the Wurster tube and the mean values of the residence time in the Wurster tube for runs #2, 4, and 5 with varying batch sizes (partition gap 15 mm, particle VMD 1749 μm, tube length 150 mm, fluidization air flow rate 73.3 m^3/h, and atomization air flow rate 3.50 m^3/h).

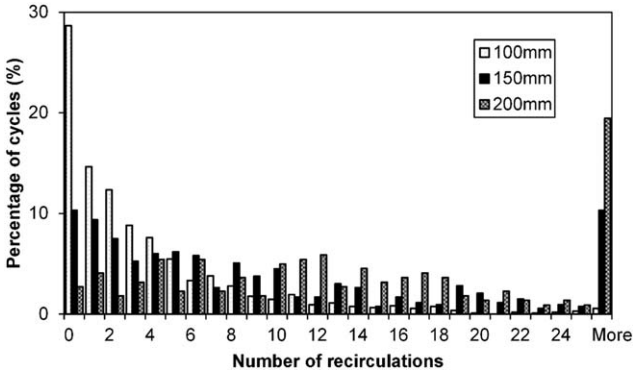

Figure 13. The number of recirculations for runs #2, 6, and 7, with varying tube lengths (partition gap 15 mm, batch size 200 g, particle VMD 1749 μm, fluidization air flow rate 73.3 m^3/h, and atomization air flow rate 3.50 m^3/h).

the increased batch size, which tends to push particles into the Wurster tube through the partition gap. In our case, the particles in the downbed region are fluidized, and there is thus no hydrostatic pressure pushing down on the particles. Instead, we argue that the increased batch size increases the flow resistance in the downbed region, which increases the air flow through the Wurster tube and decreases the air flow through the downbed region, thereby enhancing the solids flow rate. This conclusion is supported by examining the RTD in the Wurster tube as a function of batch size, as shown in Figure 12. Figure 12 demonstrates that the increased batch size from 200 to 600 g leads to more cycles of shorter residence times in the Wurster tube, with the mean value decreased from 1.34 to 0.53 s, which implies that the increased batch size does increase the acceleration of particles in the Wurster tube. This conclusion is confirmed by noting that a bigger batch size leads to a higher fountain as well as a larger percentage of ideal cycles. As the acceleration of particles in the tube is increased, the mass of particles in the tube also increases as shown in Table 4.

Effect of fluidization air flow

Table 4 also shows the effect of the fluidization air flow rate of 73.3, 65.8, and 80.3 m^3/h in runs #2, 15, and 16, respectively. A decrease in the fluidization air flow rate from 73.3 to 65.8 m^3/h results in an increase in the residence time in the Wurster tube from 1.38 to 2.71 s and an increase in the cycle time by 3.42 s. In addition, this 10% decrease in the fluidization flow rate results in a large RSD of 150% in the cycle time. The very large RSD in the cycle time indicates that the particle is trapped somewhere in the horizontal transport region. By contrast, an increase of 10% in fluidization air flow rate to 80.3 m^3/h increases the air flow rate in the Wurster tube, which increases the flow of particles through the Wurster tube and thus leads to a decrease of approximately 4 s in the cycle time.

Assuming that all air flow goes into the Wurster tube, the superficial air velocity can be estimated to 10.4 m/s, which is just a bit higher than the terminal velocity of 1749-μm particles, 7.8 m/s (see Table 1). Considering the velocity profile in laminar pipe flow,[25] however, the air velocity decreases to 7.5 m/s when the radial distance in the Wurster tube is larger than 20 mm. This estimation of the air velocity is further supported by CFD simulations of the single-phase gas flow in the fluid bed (not shown here). When particles move through this region, the drag is likely too low to carry the particles upward, and as a consequence recirculations occur. When decreasing or increasing the fluidization air flow, this region with low drag is enhanced or reduced accordingly and thus results in the decrease by 0.3% or the increase by 45.3% in the percentage of ideal cycles as presented in Table 4.

Effect of atomization air flow

When the atomization air flow rate increases, it is expected that the particles will accelerate faster in the Wurster tube and reach higher up in the fountain region. The results from runs #2, 17, and 18, in which the atomization air flow rate is varied at 3.50, 2.49, and 4.50 m^3/h, respectively, confirm this expectation. It is of interest to note that the low atomization air flow rate of 2.49 m^3/h results in lots of recirculations and a very long residence time (42 s) in the Wurster tube. At the same time, the residence time in the horizontal transport region dramatically increases from 8.2 to 90 s, when the atomization air flow rate is reduced from 3.50 to 2.49 m^3/h. A longer cycle time and residence time in

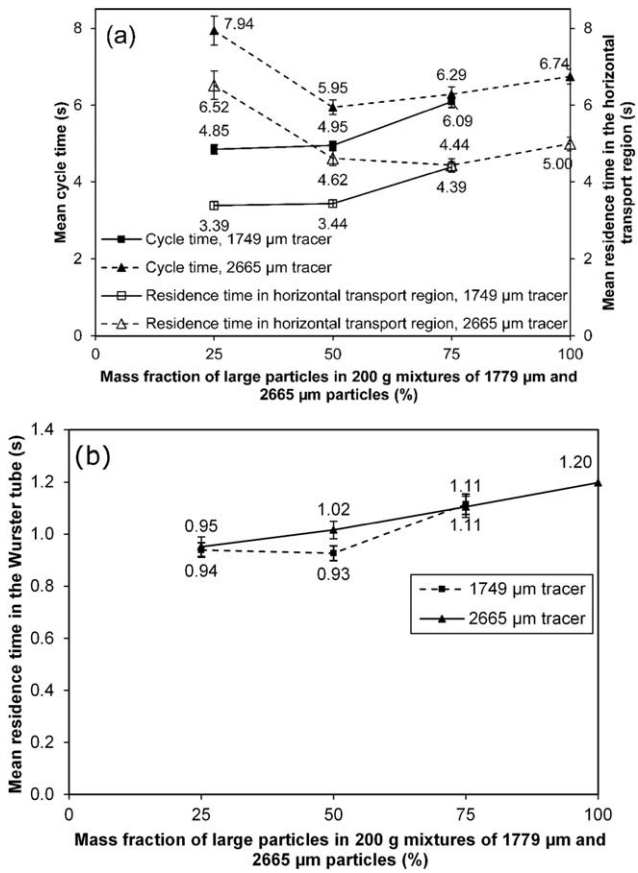

Figure 14. The mean cycle time and the mean values of the residence time in the horizontal transport region (a) and the mean values of the residence time in the Wurster tube (b) for the mixtures of 1779 and 2665 μm particles using tracer particles with diameters of 1749 and 2665 μm (partition gap 15 mm, batch size 200 g, tube length 150 mm, fluidization air flow rate 80.3 m^3/h, and atomization air flow rate 4.32 m^3/h).

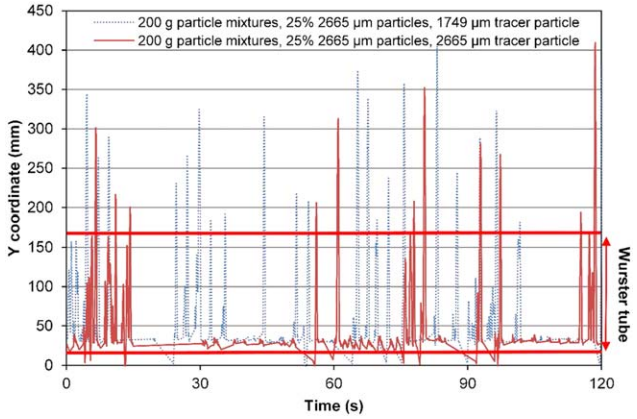

Figure 15. The axial position of the particle during 120 s for the 200 g mixtures with 25% large particles (runs #9 and 10) using tracers of 1749 and 2665 μm, respectively (partition gap 15 mm, batch size 200 g, tube length 150 mm, fluidization air flow rate 80.3 m^3/h, and atomization air flow rate 4.32 m^3/h).

[Color figure can be viewed in the online issue, which is available at wileyonlinelibrary.com.]

the tube can be expected when the atomization air flow rate decreases by simply noting that the cycle time must become infinite when the flow rate decreases below the flow rate that is required to overcome gravity in the Wurster tube.

Effect of tube length

The tube length is an important variable that affects the coating quality obtained in fluid bed equipment.[8] The most pronounced effect of increasing the tube length is the dramatic increase of number of recirculations in the Wurster tube, as illustrated in Figure 13. Increasing the tube length also results in a reduced number of ideal cycles, from 10.3 to 2.7% and an increased cycle time, from 4.97 to 24.3 s. Such a big increase in the recirculation obviously decreases the solids flow rate in the bed and thus increases the cycle time. For the sake of producing a coating thickness with a small variability, it is preferable to minimize the number of recirculations, and thus, these results imply that both the atomization and fluidization air flow rates can be optimized for each Wurster tube length. For the longer tube of 200 mm, it must be noted that the tracer particle only completed less than 250 cycles, which is not sufficient to establish a reliable mean cycle time or CTD.

Mixture of particles of different sizes

The cycle and residence times in different regions of the vessel were studied for binary mixtures of large (2665 μm) and small (1749 μm) particles. For each mixture, two experiments were carried out in order to track both a large and a small particle. Figure 14 shows the mean cycle times for mixtures of 1749 and 2665 μm particles at different mass fractions of 2665-μm particles. The results show that, at a specific weight fraction of large particles, the large particle has a longer cycle time compared to the small particle. This agrees with the findings of San José et al.[23] and Fitzpatrick et al.[14] for a Wurster coater and Chan et al.[24] for a conical spouted bed.

In Figure 14, the mean residence times in the Wurster tube and the horizontal transport region are plotted. The results show that the difference in the mean cycle times is mainly due to the difference in mean residence times in the horizontal transport region, as the mean residence times in the Wurster tube are almost the same. One explanation for the surprisingly similar residence times for both small and large particles in the Wurster tube can be that collisions between the small and large particles decrease the velocity of the small particles in the tube and increase the velocity of the large particles, resulting in a similar average residence time for all particles.

The difference in the residence time in the horizontal transport region can be understood by considering a more detailed analysis of the motion of the small and large particle, as shown in Figure 15, where the particle coordinate in the axial direction during 120 s is plotted. It is seen that the time between each cycle on average is considerably longer for the large particle, and the large particle shows a pattern of up and down movement in the horizontal transport region, which is absent for the small particle. Specifically, as shown in Figure 15 between approximately 60 and 75 s, the large particle repeatedly moves toward the bottom of the Wurster tube without being sucked into the Wurster tube. It is as if the large particle has greater difficulty to pass under the edge of the Wurster tube.

As the residence time in the Wurster tube is almost the same for both small and large particles, it is not believed that the difference in the cycle times will have an effect on the drying process in the tube. However, the difference in the residence time in the horizontal transport region will result in different numbers of passes through the spray zone and thus contribute to a difference in total amount of coating deposited on small and large particles. The data obtained here suggest that small particles possibly receive more of the coating solution, which implies that the particle size distribution can become narrower during the coating operation.

The results also show that the mean cycle time for the large particles is smallest for the mixture with equal amounts of small and large particles, and that it increases as either the fraction of large particles increases or decreases. This observation may be understood by considering the pressure drop in a packed bed. According to the Ergun equation,[26] the pressure drop in a packed bed increases as the voidage decreases and as the surface area increases. It is well known that polydispersity decreases the voidage because small particles can occupy the voids between larger particles. For binary mixtures with a size ratio of approximately 0.7, as in the present case, it has been shown (see e.g., Sohn and Moreland,[27] Yu et al.,[28] and Finkers and Hoffmann[29]) that the voidage is at a minimum when small and large particles are mixed in approximately equal amounts. One would thus expect, as observed in Figure 14, the greatest pressure drop across the downbed and horizontal transport regions and the shortest cycle time for the mixture with 50% large particles. Of course, a larger fraction of large particles decreases the surface area, but for the present particle mixtures, it can be shown that the effect of the voidage is more important and that a greater pressure drop therefore is obtained for the 50-50 mixture.

Implications for design and operation

In this section, we will discuss the results obtained from the present laboratory-scale Wurster bed in a wider perspective that may provide useful insight into the design and operation of fluid beds in general with emphasis on fluid bed coating.

First, the present results indicate that, for a given piece of equipment, there is an optimum value of the partition gap at which the gap is small enough to direct the fluidization flow

into the Wurster tube and large enough not to limit the solids flux into the tube. Obviously, the exact value depends on the design of the equipment such as the hole pattern in the distributor plate. As it in general is not possible to find this value using PEPT, other techniques are required. One interesting approach is that of Chan et al.,[24] who simply collected particles in the downbed region using a net. While this technique is more practical than PEPT, although still not very practical (especially in large-scale equipment), we believe that it must be executed with great care unless initial transients are not to affect the measured mass flow rate. Alternatively, the information about the optimal partition gap can be obtained by developing a predictive CFD model, the details of which are dependent on the scale of the equipment and the computational cost. In fact, one objective of the present work is to provide a dataset for the development and validation of such models.

The effect of batch size found in this study is very interesting. The present results show that the cycle time decreases more than a factor of three when the batch size is increased from 200 to 600 g. If it is possible to simultaneously increase the spray rate by a factor of three, this result implies that a bigger batch can be coated in a shorter time. This behavior is not observed in practice as such a large increase in the spray rate would most likely result in agglomeration, as observed by Cahyadi et al.[30] In addition, drying processes at the particle level, such as drying of polymer films or crystallization of the drug substance, may also limit the spray rate and thus preclude operation at higher spray rates. Nevertheless, the results presented here suggest that there may be opportunities to establish more efficient processes by exploring higher spray rate for bigger batches. This can also be explored using CFD, although a computational study in this case is quite difficult as it must account for drying processes on the level of the pellet as well as for agglomeration. Increasing the batch size may of course also have other effects. For example, Yang et al.[31] noted that coated pellets from a bigger batch had smoother surfaces compared to those from a smaller batch. The same researchers also found that the increase in batch size did not have any significant effect on the release profiles. In contrast, Marucci et al.[32] stated that a larger fraction of pellets in a larger batch size received a thinner coating compared to those for a smaller batch size, probably due to the electrostatic charges built up on the pellets. While our results show that increasing the batch size decreases the cycle time, it is important to remember that the residence time in the spray zone also plays a major role in determining the amount of coating received per pass. The results thus suggest that further work on the effect of the batch size are of interest.

The observed decrease in cycle time with increase in fluidization air flow rate agrees with the findings by Mann and Crosby[11] and Shelukar et al.[9] Also, the increase in the number of ideal cycles at the high fluidization air flow rate reveals that it is preferable to supply a fluidization air flow that makes the air velocity in the Wurster tube higher than the terminal velocity of particles. Of course, the motion of the air and the particles does not depend only on the fluidization flow rate but also on the configuration of the distributor. Our results cannot offer any advice for the design of the distributor plate, although, as already noted, its design will obviously affect the optimal value of the partition gap.

The atomization air flow has a strong effect on the particle motion in the Wurster tube, although small effect on the general movement of particles.[33] The present results show a positive effect of increasing the number of ideal cycles and decreasing the cycle time with an increase in the atomization air flow rate. As a nozzle of 5 mm diameter, which is larger than its usual size, was used for the convenience of computational studies, the effect of atomization air flow might be less applicable to other fluid beds with a real nozzle. Also, due to the difficulty in detecting the tracer particle in the lower region of the bed, the information on residence time in the spray zone was absent. Nevertheless, the result still provides valuable information for computational studies that will deliver the residence time in the spray zone.

The cycle times of mixtures show that large particles have longer cycle times than small particles, which indicates that smaller particles get coated more frequently. Nevertheless, in previous work,[30,32,34,35] it is shown that large particles receive higher total coating mass than small particles, likely due to the fact that large particles circulate more often or that large particles receive more coating when they pass through the spray zone. In this study, the result strongly supports the latter effect. Consider the growth model of pellets during coating for the same amount of coating and batch size, large particles are then expected to grow faster than small particles. Actually, it has been noted by Wesdyk et al.[36] that large particles demonstrated larger variance in the film thickness than small particles, because they have larger specific surface area. This effect will spread the particle-size distribution that is undesired for the production process. Knowing this difference of small and large particles, it is possible to mimic the particle-size fraction/distribution at the start of coating that perhaps exhibits the coating thickness with a small variability in the product.

Conclusions

A series of PEPT experiments to study particle motion in a Wurster fluid bed have been carried out. The measured particle trajectories were used to identify particle cycles and to determine the CTD and the RTD in different regions of the vessel. The reliability of the results was evaluated by examining the effects of the run time and the sampling interval. Experiments were carried out to evaluate the effect of the partition gap, the atomization flow rate, the batch size, and the Wurster tube length on the cycle times and RTDs. In addition, binary mixtures of different size particles were studied.

The experiments show that particles on average spend approximately 12–29% of the cycle time in the Wurster tube and most of the time in the horizontal transport region toward the bottom of the vessel. The experiments also show that particles tend to recirculate in the Wurster tube and sneak out from below the tube, particularly if the partition gap is large, the atomization flow rate is low or the Wurster tube is long. It was found that recirculation can be decreased by selecting the operating conditions appropriately or via equipment design.

The experiments also show that the cycle time decreases as the batch size increases. This decrease in the cycle time with an increase in the batch size is accompanied by an increase in the solids flow rate. In fact, the fractional increase in the solids flow rate was found to be bigger than the fractional increase in the batch size, which implies that the time to coat a batch of pellets is shorter for a bigger batch size (provided of course that it is possible to spray with a higher rate). The results also show that the CTD becomes narrower as the batch size increases, which implies that a bigger batch size will yield a product with a higher quality.

For binary mixtures of particles with a VMD of 1795 and 2665 μm, it is found that small particles have a shorter cycle time than large particles. This fact implies that small

particles get coated more frequently. It is also found that the cycle time reaches a minimum for mixtures with approximately equal amounts of small and large particles and that the cycle time is greater if the fraction of large particles is either increased or decreased. It is shown that this may be explained by considering the voidage in the downbed and horizontal transport regions. The mixture of particles has a smaller voidage and thus a larger pressure drop in the downbed and horizontal transport regions. This larger pressure drop increases the flow rate through the Wurster tube and decreases the flow rate in the downbed and horizontal transport regions, which results in a shorter cycle time.

Ongoing work on modeling of the process will give a deeper insight into the gas flow as well as the particle movement. As the variability in coating thickness is not only determined by the CTD, as indicated by the results in this study, but also the coating-per-pass distribution because of the sheltering effects in the spray zone,[3] future attention will also be paid to the study of the spray zone.

Acknowledgments

This work is undertaken within the EU seventh framework program, the PowTech Marie Curie Initial Training Network (Project no. EU FP7-PEOPLE-2010-ITN-264722). The experiments were financially supported by AstraZeneca R&D. The authors would like to thank Dr. Bindhu Gururajan for kicking off the collaboration with the Positron Imaging Centre at Birmingham University and Dr. Sven Karlsson from Swerea IVF AB, Brita Sjöblom and Hanna Matic at AstraZeneca R&D for helping preparing the materials.

Literature Cited

1. Wurster DE. Air-suspension technique of coating drug particles. A preliminary report. *J Am Pharm Assoc (Wash)*. 1959;48(8):451–454.
2. Teunou E, Poncelet D. Batch and continuous fluid bed coating–review and state of the art. *J Food Eng*. 2002;53(4):325–340.
3. Turton R. The application of modeling techniques to film-coating processes. *Drug Dev Ind Pharm*. 2010;36(2):143–151.
4. Christensen FN, Bertelsen P. Qualitative description of the Wurster-based fluid-bed coating process. *Drug Dev Ind Pharm*. 1997;23(5):451–463.
5. Ström D, Karlsson S, Folestad S, Niklasson Björn I, Laurell T, Nilsson J, Rasmuson A. A new device for coating single particles under controlled conditions. *Chem Eng Sci*. 2005;60(16):4647–4653.
6. Karlsson S, Niklasson Björn I, Folestad S, Rasmuson A. Measurement of the particle movement in the fountain region of a Wurster type bed. *Powder Technol*. 2006;165(1):22–29.
7. Mann U. Analysis of spouted-bed coating and granulation. 1. Batch operation. *Ind Eng Chem Process Des Dev*. 1983;22(2):288–292.
8. Cheng XX, Turton R. The prediction of variability occurring in fluidized bed coating equipment. I. The measurement of particle circulation rates in a bottom-spray fluidized bed coater. *Pharm Dev Technol*. 2000;5(3):311–322.
9. Shelukar S, Ho J, Zega J, Roland E, Yeh N, Quiram D, Nole A, Katdare A, Reynolds S. Identification and characterization of factors controlling tablet coating uniformity in a Wurster coating process. *Powder Technol*. 2000;110(1):29–36.
10. Turton R. Challenges in the modeling and prediction of coating of pharmaceutical dosage forms. *Powder Technol*. 2008;181(2):186–194.
11. Mann V, Crosby E. Cycle time distribution measurements in spouted beds. *Can J Chem Eng*. 1975;53(5):579–581.
12. San José MJ, Alvarez S, Peñas FJ, García I. Cycle time in draft tube conical spouted bed dryer for sludge from paper industry. *Chem Eng Sci*. 2013;100:413–420.
13. Karlsson S, Rasmuson A, van Wachem B, Björn IN. CFD modeling of the Wurster bed coater. *AIChE J*. 2009;55(10):2578–2590.
14. Fitzpatrick S, Ding Y, Seiler C, Lovegrove C, Booth S, Forster R, Parker D, Seville J. Positron emission particle tracking studies of a wurster process for coating applications. *Pharm Technol*. 2003;27(9):70–78.
15. Barigou M, Fairhurst PG, Fryer PJ, Pain JP. Concentric flow regime of solid–liquid food suspensions: theory and experiment. *Chem Eng Sci*. 2003;58(9):1671–1686.
16. Van de Velden M, Baeyens J, Smolders K. Solids mixing in the riser of a circulating fluidized bed. *Chem Eng Sci*. 2007;62(8):2139–2153.
17. Chan WC, Seville JPK, Parker DJ, Baeyens J. Particle velocities and their residence time distribution in the riser of a CFB. *Powder Technol*. 2010;203(2):187–197.
18. Parker DJ, Broadbent CJ, Fowles P, Hawkesworth MR, McNeil P. Positron emission particle tracking - a technique for studying flow within engineering equipment. *Nucl Instrum Methods Phys Res A*. 1993;326(3):592–607.
19. Parker DJ, Allen DA, Benton DM, Fowles P, McNeil PA, Tan M, Beynon TD. Developments in particle tracking using the Birmingham Positron Camera. *Nucl Instrum Methods Phys Res A*. 1997;392(1–3):421–426.
20. Parker DJ, Forster RN, Fowles P, Takhar PS. Positron emission particle tracking using the new Birmingham positron camera. *Nucl Instrum Methods Phys Res A*. 2002;477(1–3):540–545.
21. Wang LK, Heng PWS, Liew CV. Online monitoring of particle mass flow rate in bottom spray fluid bed coating—development and application. *Int J Pharm*. 2010;395(1–2):215–221.
22. Palmer S, Ingram A, Fan X, Fitzpatrick S, Seville J. Investigation of the Sources of Variability in the Wurster Coater: Analysis of Particle Cycle Times using PEPT. Paper presented at: The 12th International Conference on Fluidization-New Horizons in Fluidization Engineering 2007; Vancouver, Canada.
23. San José MJ, Olazar M, Alvarez S, Izquierdo MA, Bilbao J. Solid cross-flow into the spout and particle trajectories in conical spouted beds. *Chem Eng Sci*. 1998;53(20):3561–3570.
24. Chan LW, Tang EK, Heng PS. Comparative study of the fluid dynamics of bottom spray fluid bed coaters. *AAPS PharmSciTech*. 2006;7(2):E45–E53.
25. Munson BR, Young DF, Okiishi TH. *Fundamentals of Fluid Mechanics*. New York: Wiley; 1990.
26. Ergun S. Fluid flow through packed columns. *Chem Eng Prog*. 1952;48(2):89–94.
27. Sohn HY, Moreland C. The effect of particle size distribution on packing density. *Can J Chem Eng*. 1968;46(3):162–167.
28. Yu A-B, Standish N, McLean A. Porosity calculation of binary mixtures of nonspherical particles. *J Am Ceram Soc*. 1993;76(11):2813–2816.
29. Finkers HJ, Hoffmann AC. Structural ratio for predicting the voidage of binary particle mixtures. *AIChE J*. 1998;44(2):495–498.
30. Cahyadi C, Koh JJS, Loh ZH, Chan LW, Heng PWS. A feasibility study on pellet coating using a high-speed quasi-continuous coater. *AAPS PharmSciTech*. 2012;13(4):1276–1286.
31. Yang ST, Van Savage G, Weiss J, Ghebre-Sellassie I. The effect of spray mode and chamber geometry of fluid-bed coating equipment and other parameters on an aqueous-based ethylcellulose coating. *Int J Pharm*. 1992;86(2–3):247–257.
32. Marucci M, Holmgren A, Carlsson H, Jarke A, Johansson M, von Corswant C. Non-uniformity of pellets coating, effect on the dose release profile and how to improve the coating process by reducing the electrostatic charging of the pellets. *Chem Biochem Eng Q*. 2012;26(4):379–384.
33. Fries L, Antonyuk S, Heinrich S, Palzer S. DEM–CFD modeling of a fluidized bed spray granulator. *Chem Eng Sci*. 2011;66(11):2340–2355.
34. Sudsakorn K, Turton R. Nonuniformity of particle coating on a size distribution of particles in a fluidized bed coater. *Powder Technol*. 2000;110(1–2):37–43.
35. Paulo Filho M, Rocha SCS, Lisboa ACL. Modeling and experimental analysis of polydispersed particles coating in spouted bed. *Chem Eng Process Process Intensif*. 2006;45(11):965–972.
36. Wesdyk R, Joshi YM, De Vincentis J, Newman AW, Jain NB. Factors affecting differences in film thickness of beads coated in fluidized bed units. *Int J Pharm*. 1993;93(1–3):101–109.

Manuscript received May 9, 2014, and revision received Nov. 10, 2014.